Vibration-rotation emission spectra and combined isotopomer analyses for the coinage metal hydrides: CuH & CuD, AgH & AgD, and AuH & AuD

Jenning Y. Seto, Zulfikar Morbi,[a] Frank Charron, Sang K. Lee,[b] Peter F. Bernath and Robert J. Le Roy[c]
Guelph-Waterloo Centre for Graduate Work in Chemistry and Biochemistry, University of Waterloo, Waterloo, Ontario N2L 3G1, Canada

(Received 1 March 1999; accepted 1 April 1999)

High resolution infrared emission spectra have been measured for AuH and AuD and for two isotopomers of each of CuH, CuD, AgH, and AgD. The molecules were made in a carbon tube furnace (King furnace), and in spite of intense background thermal emission from the furnace (at $>2000\,^{\circ}\mathrm{C}$), vibration–rotation emission data could be recorded. Together with high resolution measurements taken from the literature, the data for each species were treated using two types of combined-isotopomer analysis: One based on fits to empirical molecular parameters, and the other based on direct fits to the underlying potential energy functions, both of which take account of mass-dependent Born–Oppenheimer breakdown correction terms. Accurate isotopically related Dunham parameters and Born–Oppenheimer breakdown parameters are obtained for each species, as well as accurate analytic potential functions and adiabatic and nonadiabatic radial correction functions. © *1999 American Institute of Physics.* [S0021-9606(99)02224-2]

I. INTRODUCTION

There is considerable experimental and theoretical interest in the spectra of metal-containing diatomic hydride molecules. This is due partly to the importance of transition metal hydrides in heterogeneous catalysis,[1] and partly to their presence in many astronomical sources.[2] They are also ideal systems for studying the breakdown of the Born–Oppenheimer approximation and first-order semiclassical quantization condition, which in turn cause simple first-order semiclassical mass-scaling of Dunham or band constants to fail to predict accurately the energy level differences among different isotopomers. These effects are particularly large for hydride molecules[3–5] and for the high rotational levels observed in high temperature emission spectroscopy experiments. These considerations led us to undertake a series of high resolution infrared emission studies of the spectra of the coinage metal hydrides.

Since the first laboratory study of CuH in 1923,[6] the visible and vacuum ultraviolet (UV) spectra of CuH and CuD have been studied extensively by many investigators. The $A\,^1\Sigma^+-X\,^1\Sigma^+$ transition of CuH has been observed in sunspot spectra[7] and tentatively identified in the spectrum of the star 19 Piscium.[8] To date, the most comprehensive work has been carried out by Ringström, who observed five excited electronic states, $A\,^1\Sigma^+$, $b\Delta_2$, $B\,^3\Pi_{0^+}$, $C1$, and $c1$ in the 3300–3900 Å region,[9] and the $E\,^1\Sigma^+-X^1\Sigma^+$ transition in the 2744–2270 Å region.[10] Other work includes studies by Grundström,[11] who analyzed the $D\,^1\Sigma^+-X^1\Sigma^+$ transition in the 2260–2228 Å region, and more recently by Brown and Ginter[12] who recorded absorption spectra from 2500–1750 Å. Along with the reanalysis of the $E-X$ and $D-X$ systems, they found four new transitions: $F\,1^{\pm}-X\,^1\Sigma^+$, $G\,0^+-X\,^1\Sigma^+$, $H\,1^{\pm}-X\,^1\Sigma^+$, and $I\,1^{\pm}-X\,^1\Sigma^+$. These states are labeled using Hund's case (c) notation. All of these excited states exhibit perturbations, and the H and I states also show signs of predissociation. Although the visible spectrum of CuD has not been as extensively studied as that for CuH, the $A\,^1\Sigma^+-X\,^1\Sigma^+$ system was recorded by Heimer,[13] Jeppesen,[14] Ringström,[9] and most recently by Fernando *et al.*[15] using FT (Fourier transform) emission spectroscopy using a hollow cathode discharge.

In the infrared, the vibration–rotation spectrum of the ground state of CuH was accidentally observed by Ram *et al.*[16] A copper hollow cathode lamp was used in an experiment with a continuous flow of Ne and H_2 gases to record the spectrum of NeH^+.[16] Copper atoms were sputtered off the cathode material, and in the presence of H_2 the CuH molecule was formed.[17] The 1–0, 2–1 bands and the 2–0 overtone band of ^{63}CuH and ^{65}CuH were recorded with a Fourier-transform spectrometer at 0.05 cm^{-1} resolution in the 1800–5000 cm^{-1} region. However, those measurements are superceded by the ones reported herein.

Evenson and co-workers[18,19] were able to generate ^{63,65}CuH and ^{63,65}CuD in a long hollow cathode discharge, and to measure their pure rotational spectra by tunable far-infrared spectroscopy. The pure rotational transitions were probed by mixing mid-infrared radiation from two CO_2 lasers (ν_1 and ν_2) and a microwave source (ν_μ). The resulting far infrared radiation ($\nu_{\mathrm{FIR}}=|\nu_1-\nu_2|\pm\nu_\mu$) was passed through the cell and pure rotational transitions of $X\,^1\Sigma^+$ (v

[a]Present address: Division of Geological and Planetary Science, California Institute of Technology, M/C 170-25, Pasadena, CA 91125.
[b]Present and permanent address: Department of Chemistry, Pusan National University, Kumjeong-ku, Pusan 609-735, Korea.
[c]Electronic mail: leroy@uwaterloo.ca

 © 1999 American Institute of Physics

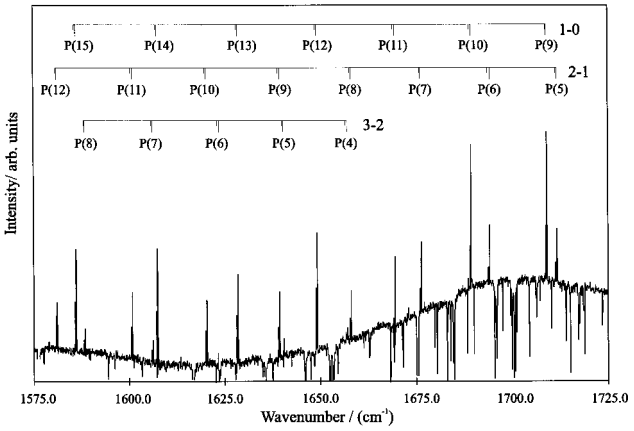

FIG. 1. A portion of the spectrum of CuH in the *P*-branch region; the absorption lines are due to H_2O present as an impurity the furnace.

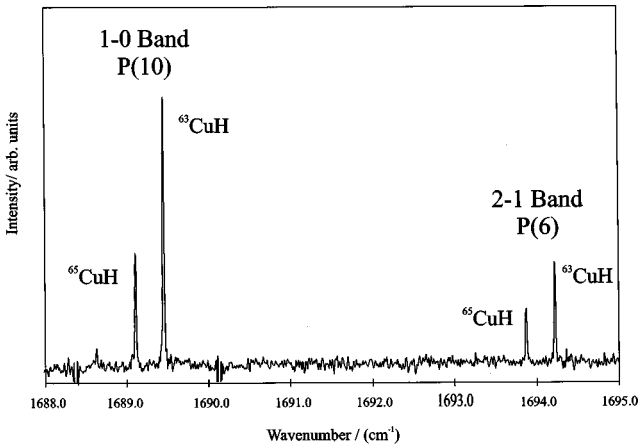

FIG. 2. A part of the spectrum of CuH showing the isotopic shift between ^{63}CuH and ^{65}CuH.

$=0$) were recorded from $J=2\leftarrow1$ to $J=11\leftarrow10$ for ^{63,65}CuH, from $J=3\leftarrow2$ to $J=19\leftarrow18$ for ^{63}CuD, and from $J=3\leftarrow2$ to $J=16\leftarrow15$ for ^{65}CuD.[18,19] In addition, Okabayashi and Tanimoto[20] have reported accurate measurements of the $J=1\leftarrow0$ transitions of ^{63,65}CuH. All of these pure rotational transitions were included in the present data analyses.

Spectra of AgH were first measured in 1931,[21] and subsequent classical work was summarized by Huber and Herzberg.[22] More recently there have been two infrared diode laser experiments. The Jones group measured 21 rovibrational transitions of the 1–0, 2–1, and 3–2 bands for ^{107,109}AgH and 33 transitions for the same bands of ^{107,109}AgD.[23,24] On the other hand, theoretical studies of these molecules have been numerous, at least partly because relativistic effects are important for quantitative calculation of the properties of molecules formed from atoms as heavy as Ag. For example, in one of the best relativistic calculations to date, Ziegler *et al.*[25] obtained a vibrational frequency of $\omega_e=1709$ cm^{-1} and an equilibrium bond length of $R_e=1.61$ Å, while their nonrelativistic calculation gave $\omega_e=1605$ cm^{-1} and $R_e=1.71$ Å. Comparisons with the experimental results show that the former are much closer to the truth.

The most comprehensive experimental study of AuH and AuD was the absorption measurements of Ringström in the 2200–3000 Å region.[26,27] He identified five excited electronic states, four of which display Hund's case (c) coupling. These states were found to have large equilibrium internuclear distances and small dissociation energies, as well as many perturbations. However, the limited resolution of those results means they can provide little information about Born–Oppenheimer breakdown effects, so they were not included in the present analysis. On the other hand, Fellows *et al.*[28] recently recorded high resolution optical spectra of the $A\,0^+\rightarrow X\,^1\Sigma^+$ system of AuH using a Fourier transform spectrometer, and their data were included in the analysis of the new infrared measurements reported herein.

Although little studied experimentally, there have been numerous theoretical studies of AuH and AuD. This is because, as with silver, molecules formed from gold are useful for studying the influence of relativistic effects on atomic and molecular properties.[29,30] For example, nonrelativistic calculations[31] predict the wrong energy order for the first two excited states of the Au atom, ^2P and ^2D, while relativistic calculations agree well with experiment.[32] Calculations have been carried out on the $X\,^1\Sigma^+$ ground state of AuH in order to study the effect of relativity on the bond length,[33] the energy ordering of low-lying electronic states,[34] the ionization energy,[35] and the dipole[36] and quadrupole moments.[37]

II. EXPERIMENT

The infrared emission spectra of the coinage metal hydrides were recorded with a Bruker IFS 120 HR Fourier-transform spectrometer. In these experiments, a very high temperature carbon tube furnace was employed to melt and vaporize the coinage metals. This furnace, sometimes called a King furnace, is 0.5 m in length and the central section of the tube has a 40 mm inner diameter. The tube windows are 1″ (25.4 mm) in diameter and the tube bore diameter for the outer sections is 15 mm. The furnace is heated by a power supply (Astra Industries), and the temperature is controlled by manually adjusting the current fed to the heating elements. The temperature was measured with an optical pyrometer by sighting on the thermal emission down the center of the tube. Although this method is imprecise, an accurate temperature measurement would require a clear view of the furnace wall, and this is not possible with the present experimental arrangement. These measured temperatures are, therefore, lower bounds to the real values. The windows and the outer jacket of the furnace are cooled by a flow of water with a liquid–liquid heat exchanger and recirculator.

In the Cu experiments, a small piece of Cu rod ($\sim$5 g) was placed inside the central section of the furnace in a carbon boat. The furnace was rapidly heated to $\sim$1500 °C and a flow of H_2 or D_2 gas was continuously maintained through the tube. For the CuH experiment, the total pressure inside the tube was $\sim$120 Torr and the spectrum was recorded by coadding 10 scans at 0.02 cm^{-1} resolution. The instrumental parameters for the spectrometer were: A CaF_2 beamsplitter, liquid N_2 cooled HgCdTe [(MCT) mercury cadmium tellu-

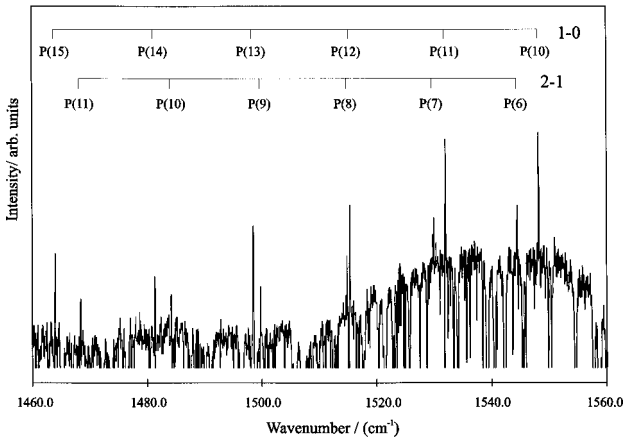

FIG. 3. A portion of the *P*-branch spectrum of AgH. Strong absorption lines are due to H_2O.

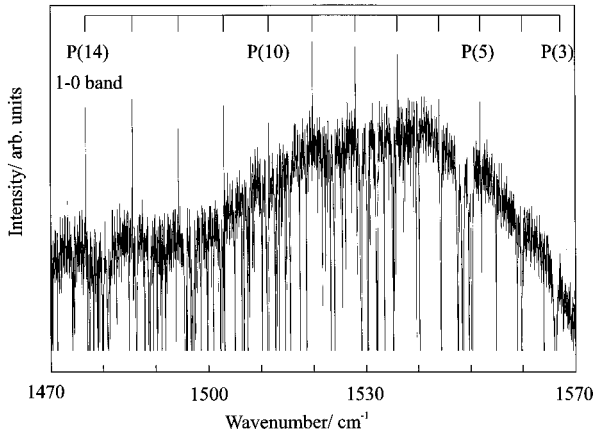

FIG. 5. A portion of the AuD spectrum; the signal to noise is very low for the AuD transitions (5:1 for the best lines) in this spectrum.

ride] detector, and KRS–5 (thallium bromoiodide) windows on the external emission port of the spectrometer. The spectrum was recorded at a temperature exceeding 1700 °C (and probably exceeding 2000 °C) in the 1300–2100 cm^{-1} wave number range.

The silver experiments were performed by placing a few grams cut from a silver ingot in a carbon boat inside the furnace. For the experiments with gold, a single troy ounce of 99.9% purity gold was purchased locally from the Canadian Imperial Bank of Commerce (Johnson & Matthey). The CuH and CuD experiments were performed on different days, as were the AgH and AgD measurements, while the AuH and AuD experiments were performed on the same day. In the latter experiments, 0.5 troy ounce of Au was placed inside the furnace and melted, first under an atmosphere of D_2 gas to record the AuD spectrum, and subsequently with H_2 gas to record the spectrum of AuH. Sample spectra of all these species are shown in Figs. 1–5. The rotational constants for the coinage metal hydrides are fairly large ($\geqslant 3.2$ cm^{-1}), so each rotational line is well isolated (line spacing $\sim 2B$ near the origin). The signal-to-noise ratio for the CuH and CuD was ~40:1 for the best lines, giving a measurement precision of ± 0.001 cm^{-1} for most lines. Although the signal-to-noise ratio for AgH and AgD was much poorer, ~10:1, the measurement precision in the more intense (lower–v) bands was also ± 0.001 cm^{-1} for the best lines. The estimated precision of most lines in the first two bands of each of AuH and AuD was also about ± 0.001 cm^{-1}. Both the AuD and AgH emission spectra are overlapped with strong absorption lines of H_2O, leading to blending of some rotational lines, but the H_2O lines also provide an absolute calibration of the spectrum. The AgD spectrum did not overlap with any other spectral features, while that for AuH was overlapped with strong CO_2 emission lines.

The new infrared line positions were measured by fitting a Voigt line shape function to each feature using J. Brault's data reduction program PC-DECOMP. It determines the center of a line by fitting its profile to a Voigt line shape function, which is a convolution of Gaussian and Lorentzian functions.[38] To assign the lines in each spectrum we used an interactive color Loomis–Wood program written by C. N. Jarman which allows one visually to pick out a series of rotational lines belonging to a vibrational band. Where available, ground state combination differences (for CuH/D from Refs. 18 and 19, for AgH/D from Refs. 23 and 24) were then used to correctly assign the spectra.

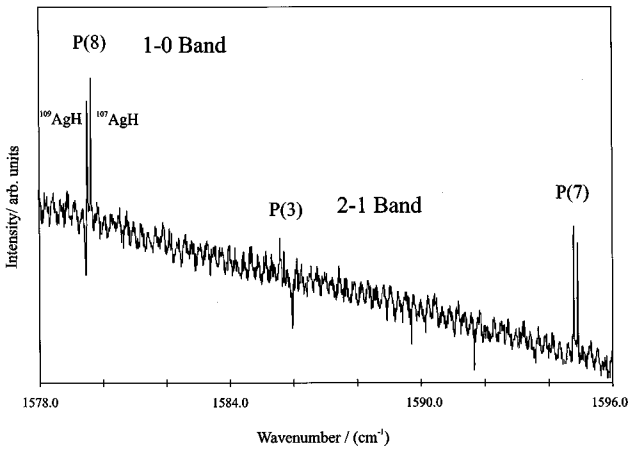

FIG. 4. A portion of the spectrum of AgH showing the small isotopic shift between ^{107}AgH and ^{109}AgH.

III. ANALYSIS

In all of the fits reported herein, the observed transition energies were weighted by the inverse square of their uncertainties, and the quality of fit is indicated by the value of dimensionless standard error[39]

$$\overline{\sigma}_f = \left\{ \frac{1}{N-M} \sum_{i=1}^{N} \left[\frac{y_{\mathrm{calc}}(i) - y_{\mathrm{obs}}(i)}{u(i)} \right]^2 \right\}^{1/2}, \tag{1}$$

where each of the N experimental data $y_{\mathrm{obs}}(i)$ has an uncertainty of $u(i)$, and $y_{\mathrm{calc}}(i)$ is the value of datum–i predicted by the M–parameter model being fitted. All parameter uncertainties quoted here are 95% confidence limit uncertainties, and the atomic masses used in the combined isotope analysis were taken from the 1993 mass table.[40]

A. Data Used in the Analysis

For the copper hydride system the new infrared data at the core of the present analysis consists of the (1,0), (2,1), (3,2), and (4,3) bands of ^{63}CuH and the (1,0), (2,1), and (3,2) bands of ^{65}CuH, ^{63}CuD, and ^{63}CuD. For strong unblended lines the associated measurement uncertainty was estimated to be 0.001 cm^{-1}. In an effort to optimally characterize the X–state of this system, the present analysis also incorporated the pure rotational measurements for the $v=0$ levels of all four isotopomers,[18–20] as well as the (0,0), (0,1), and (1,0) bands of the electronic A–X systems of ^{63}CuD and ^{65}CuD reported by Fernando *et al.*[15] The uncertainties used to define the weights used for these published data were[18,19] 0.000 003 and[20] 0.000 000 5 cm^{-1} for the pure rotational transitions and 0.004 cm^{-1} for the electronic transitions.[15] While more extensive A–X data have been reported by Ringström,[9] they are of much lower accuracy, and so were not used here.

For the silver hydride system the present analysis was based solely on our new infrared data. It consists of the (1,0), (2,1), and (3,2) bands of the four isotopomers ^{107}AgH, ^{109}AgH, ^{107}AgD, and ^{109}AgD, and the average uncertainty for strong unblended lines was taken as 0.001 cm^{-1}.

For the gold hydride system our new infrared data consists of the (1,0) and (2,1) bands of ^{197}AuH and the (1,0), (2,0), and (3,2) bands of ^{197}AuD; for these measurements the uncertainty associated with strong unblended lines was estimated to be 0.001 cm^{-1}. New high resolution optical measurements of the (0,0), (1,0), (2,0), (0,1), (1,1), (2,1), and (1,2) bands of the $A(0^+)-X(^1\Sigma^+)$ system of ^{197}AuH reported by Fellows *et al.*,[28] with estimated uncertainties of 0.003 cm^{-1}, were also included in this analysis.

Listings of the data sets used in the present analyses may be obtained by sending requests by electronic mail to either P.F.B. (bernath@UWaterloo.ca) or R.J.L. (leroy@UWaterloo.ca), or from the AIP E-PAPS electronic database.[41]

B. Combined isotopomer Dunham-type analysis

1. The method

The first stage of the analysis consisted of fitting to a separate Dunham expansion for each isotopomer of each species. In all cases, the residual discrepancies were comparable to the experimental uncertainties, and the internal consistency of the fits showed that there were no mis-assignments or anomalies in these data sets. However, the total numbers of parameters required to represent the various data sets was rather large.

In order to simplify the representation of these multi-isotopomer data sets and to extract physically interesting information about Born–Oppenheimer breakdown effects, all of the multi-isotopomer data for each system were then refitted using a combined-isotopomer Dunham-type expression for the level energies. Following Ref. 42, observed transitions for isotopomer-α of species A–B formed from atoms of mass M_A^α and M_B^α were expressed as differences between level energies written as

$$E^\alpha(v,J)=\sum_{(l,m)\neq(0,0)} Y_{l,m}^1\left(\frac{\mu_1}{\mu_\alpha}\right)^{m+l/2}(v+1/2)^l[J(J+1)]^m + \sum_{(l,m)\geqslant(0,0)}\left\{\frac{\Delta M_A^\alpha}{M_A^\alpha}\delta_{l,m}^A+\frac{\Delta M_B^\alpha}{M_B^\alpha}\delta_{l,m}^B\right\} \times\left(\frac{\mu_1}{\mu_\alpha}\right)^{m+l/2}(v+1/2)^l[J(J+1)]^m, \quad (2)$$

where $\Delta M_A^\alpha = M_A^\alpha - M_A^1$, and $\alpha=1$ (as in $Y_{l,m}^1 \equiv Y_{l,m}^{\alpha=1}$) identifies the selected reference isotopomer, which in the present work is always the hydride of the most abundant isotope of the metal. This expression is fundamentally equivalent to the familiar Ross–Eng–Kildal–Bunker–Watson[43–45] expansion, except that the Born–Oppenheimer and JWKB breakdown terms are included as additive rather than multiplicative corrections, the reference species is a real isotopic molecule, and $Y_{0,0}$ is included properly. Unlike the conventional[43–45] $\{U_{l,m}\}$'s, the constants $\{Y_{l,m}^1\}$ have sensible units (cm^{-1}) and direct physical significance as the conventional Dunham constants for the reference ($\alpha=1$) isotopomer. The analogous constants for other ($\alpha\neq1$) isotopomers are readily generated from

$$Y_{l,m}^\alpha=\left\{Y_{l,m}^1+\frac{\Delta M_A^\alpha}{M_A^\alpha}\delta_{l,m}^A+\frac{\Delta M_B^\alpha}{M_B^\alpha}\delta_{l,m}^B\right\}\left(\frac{\mu_1}{\mu_\alpha}\right)^{m+l/2}. \quad (3)$$

Other advantages of this expansion are discussed elsewhere.[42]

Within this formalism, the choice of an actual molecular species (isotopomer-1) as the reference system means that by definition $Y_{0,0}^1\equiv0$. The analogous terms for other isotopomers are in general nonzero, since the Jeffreys–Wentzel–Kramers–Brillouin (JWKB) and Born–Oppenheimer breakdown corrections give rise to small nonzero $\delta_{0,0}^A$ coefficients. Unfortunately, the latter cannot be determined empirically if the available data involve only a single electronic state. However, for transitions between different electronic states, $S_2\leftrightarrow S_1$, if sufficiently accurate data are available for different isotopomers one can empirically determine the electronic isotope shift

$$\delta Y_{0,0}^\alpha=\left\{\frac{\Delta M_A^\alpha}{M_A^\alpha}[\delta_{0,0}^A(S_2)-\delta_{0,0}^A(S_1)] + \frac{\Delta M_B^\alpha}{M_B^\alpha}[\delta_{0,0}^B(S_2)-\delta_{0,0}^B(S_1)]\right\}. \quad (4)$$

In practice this means that the second sum in Eq. (2) should only include the $(l,m)=(0,0)$ term for the second and higher of the electronic states considered, and that the coefficients actually determined in the fit are the *differences* between the ''real'' $\delta_{0,0}^A$ values for the two electronic states

$$\tilde{\delta}_{0,0}^A(S_2)=\delta_{0,0}^A(S_2)-\delta_{0,0}^A(S_1). \quad (5)$$

The fact that it naturally yields this explicit description of electronic isotope shifts is another advantage of the formalism of Eq. (2).

TABLE I. Parameters for the $X\,^1\Sigma^+$ and $A\,^1\Sigma^+$ states of CuH and CuD obtained from a simultaneous fit of 754 high resolution microwave, infrared and visible transitions for all 4 isotopomers to energy differences defined by Eq. (2); the numbers in parentheses are the 95% confidence limit uncertainties in the last significant digits shown.

	All-isotopomer fit	Generated from the ^{63}CuH constants & Eq. (3)		
Constant	^{63}CuH	^{65}CuH	^{63}CuD	^{65}CuD
$X\,^1\Sigma^+$ State Constants				
$Y_{1,0}$	1941.610 45 (250)	1941.140 557	1384.521 069	1383.860 976
$Y_{2,0}$	−37.886 99 (210)	−37.868 611	−19.258 206	−19.239 825
$Y_{3,0}$	0.1923 (7)	0.192 1601	0.068 6299	0.068 5317
$Y_{4,0}$	−0.010 42 (7)	−0.010 409 89	−0.002 691 78	−0.002 686 64
$Y_{0,1}$	7.944 817 13 (820)	7.940 966 68	4.038 767 028	4.034 914 089
$Y_{1,1}$	−0.255 7021 (230)	−0.255 516 059	−0.092 684 288	−0.092 551 626
$Y_{2,1}$	0.001 4971 (160)	0.001 495 648	0.000 386 743	0.000 386 005
$Y_{3,1}$	−0.000 0585 (41)	−0.000 058 429	−0.000 010 7738	−0.000 010 7481
$Y_{4,1}$	−0.000 0057 (4)	−0.000 005 6917	−0.000 000 7484	−0.000 000 746 26
10^4 $Y_{0,2}$	−5.317 286 (270)	−5.312 1284	−1.374 200 70	−1.371 578 75
10^4 $Y_{1,2}$	0.081 76 (69)	0.081 6609	0.015 057 57	0.015 021 67
10^4 $Y_{2,2}$	−0.0018 (4)	−0.001 7974	−0.000 236 34	−0.000 235 66
10^4 $Y_{3,2}$	−0.000 387 (43)	−0.000 386 34	−0.000 036 225	−0.000 036 104
10^8 $Y_{0,3}$	2.4445 (35)	2.440 944	0.321 7442	0.320 8238
10^8 $Y_{1,3}$	−0.069 (6)	−0.068 883	−0.006 4588	−0.006 4372
10^8 $Y_{2,3}$	−0.009 (3)	−0.008 983	−0.000 6006	−0.000 5983
10^{12} $Y_{0,4}$	−1.63 (3)	−1.6268	−0.108 775	−0.108 361
$\delta^{Cu}_{1,0}$	0.036 (7)	⋯	⋯	⋯
10^3 $\delta^{Cu}_{0,1}$	0.118 (4)	⋯	⋯	⋯
$\delta^{H}_{1,0}$	0.8471 (40)	⋯	⋯	⋯
$\delta^{H}_{2,0}$	−0.007 (3)	⋯	⋯	⋯
$\delta^{H}_{3,0}$	−0.0058 (7)	⋯	⋯	⋯
10^3 $\delta^{H}_{0,1}$	2.9028 (42)	⋯	⋯	⋯
10^3 $\delta^{H}_{1,1}$	−0.169 (5)	⋯	⋯	⋯
10^6 $\delta^{H}_{0,2}$	−0.463 (15)	⋯	⋯	⋯
10^9 $\delta^{H}_{0,3}$	0.12 (4)	⋯	⋯	⋯
$A\,^1\Sigma^+$ State Constants				
$T_{0,0}$	[23 292.1406 (3000)]	[23 292.132 45]	23 326.025 35 (120)	23 326.028 37
$\delta Y_{0,0}$	⋯	⋯	0.0	−0.036 62
$Y_{1,0}$	[1717.543 (5200)]	[1717.126 35]	1224.476 44 (370 000)	1223.891 95
$Y_{2,0}$	[−53. (4)]	[−52.974 29]	−26.937 76 (190 000)	−26.912 05
$Y_{0,1}$	[6.929 333 (52)]	[6.926 029 98]	3.521 900 31 (2700)	3.518 568 54
$Y_{1,1}$	[−0.257 64 (10)]	[−0.257 4525]	−0.093 355 89 (3600)	−0.093 222 27
10^4 $Y_{0,2}$	[−4.647 33 (400)]	[−4.642 8222]	−1.200 5348 (10 000)	−1.198 2442
10^4 $Y_{1,2}$	[−0.066 (9)]	[−0.065 92]	−0.012 1551 (17 000)	−0.012 1261
10^8 $Y_{0,3}$	[1.833 (94)]	[1.830 33]	0.240 669 (12 000)	0.239 980
10^8 $Y_{1,3}$	[−0.8 (2)]	[−0.798 64]	−0.074 884 (21 000)	−0.074 634
10^{12} $Y_{0,4}$	[−2.2 (2)]	[−2.1957]	−0.146 81 (1700)	−0.146 25
$\tilde{\delta}^{Cu}_{0,0}$	−1.19 (4)	⋯	⋯	⋯
10^3 $\delta^{Cu}_{0,1}$	1.9 (1)		⋯	⋯
No. of data	756	110	282	228
No. parameters	38	0	0	0
$\overline{\sigma_f}$	0.849	0.864	0.741	0.977

2. Application to the coinage metal hydrides

The present combined-isotopomer parameter analyses were performed by fitting to Eq. (2) using program DSPARFIT,[42,46] which simplifies the resulting parameters by applying the sequential rounding and refitting procedure of Ref. 39. In this program, the zero of energy for each electronic state is taken to be the zero-point ($v=0,J=0$) level of the reference isotopomer ($\alpha=1$), and the electronic excitation energy determined in the fit is the difference between such zero point energies, $T_{0,0}$. The $T_{0,0}$ values for the minority isotopomers are then determined by taking account of the isotopic zero point energy differences and any Born–Oppenheimer breakdown (B–O–B) type corrections.

Fitting the present multi-isotopomer data sets for CuH, AgH, and AuH to Eq. (2) yielded the molecular constants (and uncertainties) listed in the first column of Tables I–III, respectively. These consist of the conventional Dunham constants for the reference isotopomer plus any mass-dependent or Born–Oppenheimer breakdown parameters which could be determined. These are the essential results of each analysis. For the convenience of the user, however, the remaining columns of each table list the conventional Dunham param-

TABLE II. Parameters for the $X\,^1\Sigma^+$ state of AgH and AgD obtained from a simultaneous fit of 369 high resolution infrared for all 4 isotopomers to energy differences defined by Eq. (2); the numbers in parentheses are the 95% confidence limit uncertainties in the last significant digits shown.

Constant	All-isotopomer fit	Generated from the ^{107}AgH constants & Eq. (3)		
	^{107}AgH	^{109}AgH	^{107}AgD	^{109}AgD
$Y_{1,0}$	1759.7496 (23)	1759.598 71	1250.894 68	1250.682 299
$Y_{2,0}$	−33.980 05 (150)	−33.974 223	−17.219 396	−17.213 55
$Y_{3,0}$	−0.0052 (3)	−0.005 1987	0.006 2928	0.006 2896
$Y_{0,1}$	6.450 066 (39)	6.448 9452	3.257 9187	3.256 8051
$Y_{1,1}$	−0.202 137 (35)	−0.202 087 76	−0.072 571 83	−0.072 535 86
$Y_{2,1}$	0.000 6854 (200)	0.000 685 165	0.000 174 829	0.000 174 710
$Y_{3,1}$	−0.000 1058 (37)	−0.000 105 755	−0.000 019 178 8	−0.000 019 162 6
10^4 $Y_{0,2}$	−3.467 (2)	−3.465 811	−0.884 73	−0.884 13
10^4 $Y_{1,2}$	0.047 23 (170)	0.047 2098	0.008 4529	0.008 4457
10^4 $Y_{2,2}$	−0.005 81 (98)	−0.005 8070	−0.000 748 48	−0.000 747 72
10^4 $Y_{3,2}$	0.0010 (3)	0.000 9994	0.000 091 553	0.000 091 444
10^4 $Y_{4,2}$	−0.000 16 (4)	−0.000 159 89	−0.000 010 410	−0.000 010 396
10^8 $Y_{0,3}$	1.11 (6)	1.10943	0.142 997	0.142 851
10^8 $Y_{1,3}$	−0.07 (2)	−0.06996	−0.006 409	−0.006 401
10^8 $Y_{2,3}$	−0.005 (3)	−0.004997	−0.000 3253	−0.000 3249
10^{12} $Y_{0,4}$	−1.0 (7)	−0.9993	−0.065 06	−0.064 98
10^3 $\delta^{Ag}_{0,1}$	−0.8 (7)	⋯	⋯	⋯
10^3 $\delta^{Ag}_{1,1}$	−0.15 (10)	⋯	⋯	⋯
$\delta^{H}_{1,0}$	0.8315 (52)	⋯	⋯	⋯
$\delta^{H}_{2,0}$	−0.2289 (39)	⋯	⋯	⋯
$\delta^{H}_{3,0}$	0.0455 (9)	⋯	⋯	⋯
10^3 $\delta^{H}_{0,1}$	1.23 (7)	⋯	⋯	⋯
10^3 $\delta^{H}_{1,1}$	−0.112 (19)	⋯	⋯	⋯
10^6 $\delta^{H}_{0,2}$	−0.3 (2)	⋯	⋯	⋯
10^6 $\delta^{H}_{1,2}$	−0.12 (6)	⋯	⋯	⋯
No. of data	369	79	112	99
No. parameters	25	0	0	0
$\overline{\sigma_f}$	0.977	0.951	0.927	0.942

eters for the minority isotopomers generated from the results in the first column using Eq. (3), and rounded at the first significant digit of the parameter sensitivity.[39] More significant digits are required to represent these derived constants adequately, as the compensating changes associated with the sequential rounding and refitting procedure do not come into play.[39] The $\overline{\sigma_f}$ values for the minority isotopomers seen in the last row of each table were generated by comparing predictions generated from these derived constants with the experimental data for that isotopomer alone. The magnitudes of the resulting values indicate that those derived parameters represent the data for the minority isotopomers essentially as well as would an independent fit to those data.

3. Parameter-fit results for CuH and CuD

For the copper hydride system, the only available Fourier-transform A-state data was that for the two deuteride species,[15] so no hydrogenic mass-dependent correction parameters $\delta^{H}_{l,m}$ could be determined for the A state. As a result, although the fit is parameterized with ^{63}CuH as the reference isotopomer, the A-state $Y_{l,m}$ parameters obtained for the hydride isotopomers are effectively determined from those for the ^{63}CuD by conventional first-order semiclassical mass scaling. The results for the ground state indicate that the missing hydride B–O–B type corrections will not be negligible, so these predicted hydride A-state constants are expected to be distinctly less accurate than those for the deuterides. This is indicated in Table I by the $\{Y_{l,m}\}$ values for the hydrides being placed in square brackets. Note too that while the fit is parameterized in terms of the constants for the reference isotopomer ^{63}CuH, since the only data for the A-state are those for the deuteride, the uncertainties in the $Y_{l,m}$ parameters for ^{63}CuD are listed as well. Except for small differences due to slightly different treatments of rounding, these A-state CuD constants and uncertainties are identical to those yielded by a multi-isotopomer fit to the same four-isotopomer data set which treats ^{63}CuD as the reference isotopomer.

The quantity $\delta Y_{0,0}$ for A-state CuD given in Table I is the copper electronic isotope shift implied by the fitted parameter $\tilde{\delta}^{Cu}_{0,0}(A)$. This is the absolute A-state energy shift occurring on replacing ^{63}Cu by the indicated Cu isotope in either the hydride or the deuteride. Although the analogous hydrogenic electronic isotope shift coefficient is expected to be distinctly larger than this, it cannot be determined from the data set used here, so ^{63}CuD is effectively the reference isotopomer as far as the determination of this quantity is concerned. However, it should also predict accurately the A-state electronic isotope shift from ^{63}CuH to ^{65}CuH.

A possible point of concern regarding the results in Table I is the relatively large magnitude of the uncertainties in the vibrational constants $Y_{1,0}$ and $Y_{2,0}$ for the A-state. This occurs because the experimental data for this state involved only the $v'=0$ and 1 levels of ^{63,65}CuD, and it is only the small ^{63}CuD to ^{65}CuD isotope effect which allows the determination of a vibrational anharmonicity parameter. Although

TABLE III. Parameters for the $X\ ^1\Sigma^+$ and $A\ ^1\Sigma^+$ states of AuH and AuD obtained from a simultaneous fit of 376 high resolution infrared and visible transitions for both isotopomers to energy differences defined by Eq. (2); the numbers in parentheses are the 95% confidence limit uncertainties in the last significant digits shown.

Constant	All-isotopomer fit ^{197}AuH	From the ^{197}AuH constants & Eq. (3) ^{197}AuD
$X\ ^1\Sigma^+$ State Constants		
$Y_{1,0}$	2305.500 82 (200)	1635.250 438
$Y_{2,0}$	−43.366 13 (160)	−218.188 496
$Y_{3,0}$	−0.0052 (4)	−0.001 8546
$Y_{0,1}$	7.241 538 (21)	3.642 2493
$Y_{1,1}$	−0.213 723 5 (240)	−0.076 248 707
10^4 $Y_{2,1}$	4.346 (200)	1.099 26
10^4 $Y_{3,1}$	−0.91 (5)	−0.163 232
10^4 $Y_{0,2}$	−2.8563 (8)	−0.724 1048
10^4 $Y_{1,2}$	0.022 77 (70)	0.004 084 39
10^4 $Y_{2,2}$	−0.001 54 (55)	−0.000 1959
10^4 $Y_{3,2}$	−0.0004 (1)	−0.000 036 085
10^8 $Y_{0,3}$	0.476 (10)	0.076 122
10^8 $Y_{1,3}$	−0.042 (4)	−0.001 445
$\delta^{\mathrm{H}}_{1,0}$	0.7034 (14)	⋯
$\delta^{\mathrm{H}}_{2,0}$	−0.0351 (4)	⋯
10^3 $\delta^{\mathrm{H}}_{0,1}$	1.11 (7)	⋯
10^3 $\delta^{\mathrm{H}}_{1,1}$	−0.120 (9)	⋯
10^6 $\delta^{\mathrm{H}}_{0,2}$	−1.3 (4)	⋯
10^9 $\delta^{\mathrm{H}}_{0,3}$	2.45 (81)	⋯
10^9 $\delta^{\mathrm{H}}_{1,3}$	0.52 (16)	⋯
$A\ ^1\Sigma^+$ State Constants		
$T_{0,0}$	27 344.9986 (16)	[27 437.717 14]
$Y_{1,0}$	1692.4195 (60)	[1200.219 888]
$Y_{2,0}$	−73.071 (2)	[−36.749 433]
$Y_{0,1}$	6.006 845 (130)	[3.021 009 02]
$Y_{1,1}$	−0.260 431 (220)	[−0.092 886 17]
$Y_{2,1}$	−0.020 42 (8)	[−0.005 164 96]
10^4 $Y_{0,2}$	−3.2216 (98)	[−0.814 859 6]
10^4 $Y_{1,2}$	−0.04 (2)	[−0.007 175]
10^4 $Y_{2,2}$	−0.1134 (56)	[−0.014 425 5]
10^8 $Y_{0,3}$	0.1 (2)	[0.012 721]
10^8 $Y_{1,3}$	−1.11 (19)	[−0.100 137]
10^{12} $Y_{0,4}$	−2.3 (11)	[−0.147 15]
No. of data	376	142
No. parameters	32	0
$\overline{\sigma_f}$	0.954	0.867

interparameter correlation makes these uncertainties relatively large, neglecting the anharmonic term increases $\overline{\sigma_f}$ for the global fit by nearly 50%, so it cannot be ignored. These uncertainties in turn give rise to relatively large uncertainties in the H↔D zero point energy shift, which explains the difference between the magnitudes of the uncertainties in the $T_{0,0}$ values for the H and D isotopomers. However, the actual A-state vibrational spacings $\Delta G_{1/2}$ are still quite accurately determined, particularly for the D-isotopomers, and since the main reason for including the optical data was to improve the statistics on the determination of the X-state parameters, the size of the uncertainties in these A-state vibrational parameters is not a matter of great concern.

4. Parameter-fit results for AgH and AgD

For the silver hydride system, an interesting apparent anomaly seen in Table II is the fact that the magnitude of $Y_{3,0}$ actually *increases* from the hydride to the deuteride. This counter-intuitive result is explained by the fact that the value of this constant for the reference isotopomer is unusually small, almost four orders of magnitude smaller than $Y_{2,0}$, allowing the normal mass scaling to be overwhelmed by the effect of the B–O–B correction parameter $\delta^{\mathrm{H}}_{3,0}$. As pointed out by Watson,[45] this is the type of case in which the conventional[43–45] B–O–B parameterization would give anomalously large values for its correction parameter[42]

$$\Delta^{\mathrm{A}}_{l,m} = -\delta^{\mathrm{A}}_{l,m}(M^1_{\mathrm{A}}/m_e)/(Y^1_{l,m}+\delta^{\mathrm{A}}_{l,m}+\delta^{\mathrm{B}}_{l,m}). \tag{6}$$

Applying this expression to the results in Table II yields $\Delta^{\mathrm{H}}_{3,0} = -2074.$ which is anomalously large relative to the usual magnitude of order unity for such parameters. This illustrates one of the weaknesses of the conventional Ross–Eng–Kildal–Bunker–Watson representation, which is that unusually large or small values values of the normal $Y_{l,m}$ parameters can give rise to anomalously small or large values of the $\Delta^{\mathrm{A}}_{l,m}$ correction parameters, even though the absolute magnitude of the associated B–O–B correction itself (as indicated by the present $\delta^{\mathrm{A}}_{l,m}$ parameters) may be ''normal'' (i.e., quite small).

5. Parameter-fit results for AuH and AuD

Because our high resolution infrared data set for AuH consists of only 69 lines, the 165 optical A–X data of Fellows *et al.*[28] are fairly important for the present analysis, even though they are of somewhat (up to 6 times) lower accuracy. However, the fact that no deuteride data are available for the A-state means that no mass-dependent $\delta^{\mathrm{H}}_{l,m}$ parameters may be determined for it. As a result, the predicted A-state deuteride parameters in Table III were generated by simple first-order mass scaling; as for the copper hydrides, the resulting lower accuracy is indicated by placing the associated constants in square brackets.

C. Direct potential fit analysis

1. The method

As a more compact and more physically significant alternative to the Dunham-type analysis reported above, all data for the various isotopomers of a given species were also fitted directly to eigenvalue differences numerically calculated from the effective radial Schrödinger equation

$$\left\{-\frac{\hbar^2}{2\mu}\frac{d^2}{dR^2}+V^{\alpha}_{ad}(R)+\frac{\hbar^2 J(J+1)}{2\mu R^2}\times[1+q^{\alpha}(R)]-E_{v,J}\right\}\psi_{v,J}(R)=0, \tag{7}$$

where the effective adiabatic potential for isotopomer-α in a given electronic state is written as that for isotopomer–($\alpha=1$) plus atomic mass dependent ''adiabatic'' correction terms

$$V^{\alpha}_{ad}(R)=V^1_{ad}(R)+\frac{\Delta M^{\alpha}_{\mathrm{A}}}{M^{\alpha}_{\mathrm{A}}}\Delta V^{\mathrm{A}}_{ad}(R)+\frac{\Delta M^{\alpha}_{\mathrm{B}}}{M^{\alpha}_{\mathrm{B}}}\Delta V^{\mathrm{B}}_{ad}(R), \tag{8}$$

and the (nonadiabatic) effective centrifugal distortion correction term is written as

$$q^{\alpha}(R)=\frac{M_{\mathrm{A}}^{1}}{M_{\mathrm{A}}^{\alpha}}q_{\mathrm{A}}(R)+\frac{M_{\mathrm{B}}^{1}}{M_{\mathrm{B}}^{\alpha}}q_{\mathrm{B}}(R), \tag{9}$$

where both the adiabatic potential correction functions $\Delta V_{ad}^{\mathrm{A}}(R)$ and $\Delta V_{ad}^{\mathrm{B}}(R)$, and the nonadiabatic centrifugal correction functions $q_{\mathrm{A}}(R)$ and $q_{\mathrm{B}}(R)$, are isotopomer independent.

This representation of the atomic mass dependent correction terms is equivalent to that in the Hamiltonian discussed by Watson[47] and used in numerous practical analyses,[5,48,49] except that (following Ref. 42) the reference potential is the actual effective adiabatic potential for a real isotopic ($\alpha=1$) molecular species, rather than the theoretical ''clamped nuclei'' potential obtained in the lowest order version of the Born–Oppenheimer separation.[50] While of theoretical interest, the latter cannot be calculated *ab initio* to spectroscopic accuracy, and since experimental data which spans the same range of energy for all isotopomers are rarely available, when determined empirically it will tend to have much larger uncertainties at some distances than would the actual adiabatic potential for the dominant isotopomer, $V_{ad}^{1}(R)$. Moreover, the mass scaling conventions of Ref. 42 mean that the adiabatic potential correction functions $\Delta V_{ad}^{\mathrm{A}}$ and $\Delta V_{ad}^{\mathrm{B}}$ have units cm^{-1}, and their magnitude is directly related to the magnitude of the change in the potential from one isotopomer to another, while $q_{\mathrm{A}}(R)$ and $q_{\mathrm{B}}(R)$ are dimensionless and their magnitude (relative to unity) is a direct indication of the strength of these terms. Further discussion of this representation of the B–O–B correction functions may be found in Ref. 42.

In the present work, the effective adiabatic potential for the dominant isotopomer was represented by the ''expanded morse oscillator'' (EMO) function

$$V_{ad}^{1}(R)=\mathcal{D}_e\{1-e^{-\beta(z)(R-R_e)}\}^2, \tag{10}$$

where $\mathcal{D}_e$ is the potential well depth, R_e is the equilibrium bond length, $z\equiv(R-R_e)/(R+R_e)$ and both $\beta(z)$ and the adiabatic and nonadiabatic correction functions are expressed as power series in z

$$\beta(R)=\sum_{j=0}\beta_j z^j, \tag{11}$$

$$\Delta V_{ad}^{\mathrm{A}}(R)=\sum_{j=0}u_j^{\mathrm{A}}z^j,\quad \Delta V_{ad}^{\mathrm{B}}(R)=\sum_{j=0}u_j^{\mathrm{B}}z^j, \tag{12}$$

$$q_{\mathrm{A}}(R)=\sum_{j=1}q_j^{\mathrm{A}}z^j,\quad q_{\mathrm{B}}(R)=\sum_{j=1}q_j^{\mathrm{B}}z^j. \tag{13}$$

In these expansions, the units of all $\{\beta_j\}$ coefficients are $\mathrm{Å}^{-1}$, those of the $\{u_j^{\mathrm{A}}\}$ and $\{u_j^{\mathrm{B}}\}$ coefficients are cm^{-1}, and the $\{q_j^{\mathrm{A}}\}$ and $\{q_j^{\mathrm{B}}\}$ expansion coefficients are all dimensionless.

As shown by Watson,[45] the centrifugal correction functions $q_{\mathrm{A}}(R)$ may be defined to be identically zero at R_e, so the sums in Eq. (13) start at the $j=1$ term. However, treatment of the equilibrium behavior of the adiabatic potential correction functions $\Delta V_{ad}^{\mathrm{A}}(R)$ is somewhat more complicated. Different isotopomers in a given electronic state in general have slightly different well depths; between hydrides and deuterides such differences are typically of the order of a few cm^{-1}, while the analogous changes among heavy atom isotopomers will be much smaller. In the absence of vibrational data spanning most of the potential well, one cannot expect to determine such differences empirically; this is the case for the systems considered here. As a result, the leading expansion coefficients u_0^{A} and u_0^{B} for the ground state (S_1), which determine the isotopic shift of the potential minimum, cannot be determined from fits to the available data. Thus, $u_0^{\mathrm{A}}(S_1)=u_0^{\mathrm{B}}(S_1)=0$, which means in effect that for the ground states of the coinage metal hydrides, the sums in Eq. (12) begin at $j=1$.

For an excited electronic state (S_2), the leading adiabatic correction function coefficients are related to the adiabatic electronic isotope shift

$$\Delta T_e^{\alpha}(S_2)=(\Delta M_A^{\alpha}/M_A^{\alpha})[u_0^{\mathrm{A}}(S_2)-u_0^{\mathrm{A}}(S_1)]+(\Delta M_B^{\alpha}/M_B^{\alpha})\times[u_0^{\mathrm{B}}(S_2)-u_0^{\mathrm{B}}(S_1)]. \tag{14}$$

For the present cases in which the ground state $u_0^{\mathrm{A}}(S_1)$ values cannot be determined from the existing data, by analogy with Eq. (5), the quantity actually determined from the fits as the leading adiabatic correction expansion coefficient for (excited) state-S_2 is

$$\tilde{u}_0^{\mathrm{A}}(S_2)=u_0^{\mathrm{A}}(S_2)-u_0^{\mathrm{A}}(S_1). \tag{15}$$

Note, however, that these effective electronic isotope shift coefficients $\tilde{u}_0^{\mathrm{A}}(S_2)$ are not expected to be identical to the $\tilde{\delta}_{0,0}^{\mathrm{A}}(S_2)$ values yielded by the parameter-fit analysis, since the former describe only the isotopic shift in the difference between the potential energy minima in the two electronic states, while $\tilde{\delta}_{0,0}^{\mathrm{A}}(S_2)$ also includes contributions due to difference in the degree of breakdown of the first-order semiclassical or JWKB approximation in the two states. However, the former contribution may usually be expected to dominate.

Together with most other published applications of the type of direct potential fit method described above, the present analysis overlooks the question of the limiting long-range behavior of the potential exponent function $\beta(R)$ and the B–O–B correction functions.[49,51–53] Our use of (half of) the Ogilvie–Tipping variable as our expansion parameter z, which approaches $+1$ as $R\rightarrow\infty$, does mean that our functions always approach finite values in this limit (which is not true of those reported in early applications of this approach), but the limiting asymptotic values of these functions will sometimes be physically implausible. In the present cases all such irregular long-range behavior occurs at distances far beyond the range associated with the existing experimental data, and so has no effect on the results presented here. However, a more robust approach which automatically incorporates appropriate long-range behavior is under development.[54,55]

2. Application to the coinage metal hydrides

Least-squares fits of experimental data to eigenvalue differences calculated from Eq. (7) were performed using program DSPOTFIT,[55] which uses the Numerov procedure[56] to numerically integrate Eq. (7) for the initial and final state of each transition. For all isotopomers of all three systems, this integration was performed on the interval $0.5\ \text{Å} \geqslant R \geqslant 5.0\ \text{Å}$ with a grid spacing of 5×10^{-4} Å. This sufficed to ensure that the eigenvalues used to simulate the infrared and electronic transitions were converged to better than 1×10^{-4} cm^{-1}, and those representing the microwave data (for CuH) were converged to better than 1×10^{-8}. The partial derivatives of transition energies with respect to potential energy and B–O–B correction function parameters (required for the fits) were calculated from the associated eigenfunctions using the Helmann–Feynmann theorem. The numbers of significant digits required to represent the parameters determined in the fits were minimized by application of the sequential rounding and refitting procedure of Ref. 39.

For all three systems, the available data span only a fraction of the potential well depth, so we cannot expect to determine precise $\mathcal{D}_e$ values from the present analysis. The ground state well depth of each species was, therefore, fixed at the literature value[22] of $23\,000(\pm500)$ cm^{-1} for CuH, $19\,300(\pm500)$ cm^{-1} for AgH, and $27\,200(\pm1000)$ cm^{-1} for AuH. These well depths were also taken to be the same for all X-state isotopomers, so $u_0^{\text{H}}(S_1)=u_0^{\text{M}}(S_1)=0$ (for M=Cu, A, or Au). The excited $A\,^1\Sigma^+$ electronic states of CuH and AuH involved in the present analysis dissociate to a ground state hydrogen atom and the $^2D_{5/2}$ first excited state of the metal atom. Thus, the dissociation energy for the A state is defined in terms of that for the ground state, the value of T_e, and the known[57,58] atomic excitation energy $E_M(^2D_{5/2})$:

$$\mathcal{D}_e(A)=\mathcal{D}_e(X)+E_M(^2D_{5/2})-T_e(A). \tag{16}$$

Equation (16) shows that the isotopomer dependence of T_e contributes to the isotopomer dependence of $\mathcal{D}_e(\text{A})$, but all that can actually be determined here is the isotopomer dependence of the difference $[\mathcal{D}_e(\text{A})-\mathcal{D}_e(\text{X})]$.

The parameters defining the potential energy and B–O–B correction functions determined from simultaneous fits to data for all isotopomers of each system are presented in Table IV. As above, the superscript ''M'' on the labels for the B–O–B parameters $\{u_i^{\text{M}}\}$ and $\{q_i^{\text{M}}\}$ identifies the relevant coinage metal. The potential energy function and B–O–B correction functions determined in this way are shown in Figs. 6–8. The solid portion of each curve indicates the interval spanned by the data used in the analysis for each system; this is defined as the region between the classical turning points of the highest observed vibrational level. Note that since the adiabatic correction functions $\Delta V_{ad}^{\text{A}}(R)$ characterize the *differences* between the total effective potentials for different isotopomers, the range on which they are directly determined is that associated with the data for the minority isotopomer (here the deuteride), which may be smaller than that associated with the dominant one (the hydride). In the present work this was true for the ground states of CuH and AgH, and as a result, their Δ_{ad}^{H} functions are accurately know over a slightly narrower range than is the potential itself. This difference in range is indicated on Fig. 8 by the vertical bars on the curves for those two systems, which indicate the range over which the potential itself is most accurately known. Note too that the dotted portions of the potential correction functions shown in Fig. 8 are in the extrapolation region beyond the range of the interisotopomer comparisons, so the rapid oscillations seen there may mainly represent the tendency of polynomials to extrapolate badly.

The qualitative similarity of the B–O–B corrections functions for the different coinage metals (see Figs. 7 and 8) provides reassuring evidence of their physical significance. However, it is interesting to note in Fig. 7 the very different magnitudes of the centrifugal B–O–B correction functions determined for the A and X states. The greater strength of the former is in fact expected, since this term is associated with nonadiabatic coupling with $^1\Pi$ states, and the $A\,^1\Sigma^+$ state will lie much closer to, and hence, will be more strongly affected by such excited states than will the ground state.

One problem which sometimes arises in the direct potential fit approach is that the potential obtained may behave nonphysically in the extrapolation region outside the interval on which the experimental data depend. One manifestation of this is that at small distances the exponent function $\beta(z)$ may decrease sufficiently rapidly with z that the steep repulsive wall of the analytic potential can actually turn over at very small-R. This happens to occur for the present ground state potential for CuH, which has an innerwall inflection point at $R=0.609$ Å and turns over at $R=0.475$ Å. However, these distances are far smaller than the physically accessible potential well region, since the zero of energy where the inner potential wall crosses the dissociation limit lies at $\sigma=1.026$ Å. The computer program[55] used here avoids numerical difficulties this might cause by automatically checking for such behavior, and arbitrarily fixing $\beta(z)=\beta(R=R_x)$ for $R<R_x$, where R_x is the distance ($<R_e$) where the third derivative of the potential changes sign. For our ground state potential for CuH $R_x=0.7285$ Å, and since the potential energy there is $100\,391$ cm^{-1} above the dissociation limit, this correction has no effect on any bound-state properties or calculations.

An analogous problem which also may arise sometimes is that if $\beta(z)$ in the large-R extrapolation region decreases sufficiently rapidly with R, it will give rise to a spurious outer second minimum in the potential. In the present work this happens to occur with our potentials for the X state of CuH and the A and X states of AuH.[59] However, as shown by Fig. 6, the onset of this (mis)behavior lies far beyond the region spanned by the data, and will have no practical effect on bound state property calculations. As mentioned above, a more robust approach which automatically incorporates appropriate long-range behavior is under development.[54,55]

Consideration of Tables I–IV shows that for all three molecular systems the dimensionless standard error $\overline{\sigma_f}$ for the direct potential fit was typically a few % larger than that for the Dunham-type parameter fit to the same data. This is to be expected, as the potential fit imposes a consistent physical model, while the unconstrained Dunham-type parameter fits of Tables I–III have a greater ability to follow nonphysical fluctuations in the data, so the apparent im-

TABLE IV. Potential parameters obtained on fitting all observed transition frequencies to eigenvalue differences calculated by solving Eq. (7).

Parameter	^{63}CuH	^{107}AgH	^{197}AuH
X–State Potential Parameters			
$\mathcal{D}_e$ / cm^{-1}	23 000.0 (500)[a]	19 300.0 (500)[a]	27 200.0 (1000)[a]
R_e/ Å	1.462 543 776 (240)	1.617 911 0 (27)	1.523 675 2 (13)
β_0 / Å^{-1}	1.552 828 24 (190)	1.541 581 6 (24)	1.704 802 65 (210)
β_1 / Å^{-1}	−0.061 528 (150)	0.106 52 (10)	0.052 87 (8)
β_2 / Å^{-1}	1.035 55 (65)	1.484 53 (83)	1.469 61 (100)
β_3 / Å^{-1}	1.9434 (95)	2.295 (9)	2.051 (17)
β_4 / Å^{-1}	3.313 (26)	5.38 (7)	1.35 (11)
β_5 / Å^{-1}	1.2 (5)	−1.4 (5)	−11. (1)
β_6 / Å^{-1}	−14.4 (18)	⋯	⋯
u_1^{M} / cm^{-1}	3.4 (1)	⋯	⋯
u_1^{H} / cm^{-1}	81.67 (14)	33.15 (140)	37.45 (110)
u_2^{H} / cm^{-1}	−91.3 (18)	59. (9)	116. (8)
u_3^{H} / cm^{-1}	−1057. (110)	−660. (30)	−1110. (21)
u_4^{H} / cm^{-1}	5000. (890)	⋯	⋯
u_5^{H} / cm^{-1}	−16000. (3500)	⋯	⋯
q_1^{M}	0.00 003 7 (9)	⋯	⋯
q_1^{H}	0.00 143 1 (20)	0.0001 (3)	0.0007 (1)
q_2^{H}	−0.0056 (9)	0.0115 (14)	0.0032 (6)
q_3^{H}	⋯	−0.048 (12)	⋯
A–State Potential Parameters			
T_e / cm^{-1}	23 412.2165 (180)	⋯	27 665.2587 (1700)
$\mathcal{D}_e$ / cm^{-1}	10 790.3485[b]	⋯	8696.0413[b]
R_e / Å	1.566 360 3 (39)	⋯	1.672 3027 (230)
β_0 / Å^{-1}	1.989 147 (130)	⋯	2.200 424 1 (8700)
β_1 / Å^{-1}	1.3427 (12)	⋯	1.3022 (190)
β_2 / Å^{-1}	4.59 (3)	⋯	0.9 (2)
β_3 / Å^{-1}	⋯	⋯	−11.43 (200)
$\tilde{u}_0^{\mathrm{M}}$ / cm^{-1}	−1.23 (7)	⋯	⋯
u_1^{M} / cm^{-1}	−15. (6)	⋯	⋯
q_1^{M}	−0.0088 (14)	⋯	⋯
q_1^{H}	−0.0517 (28)	⋯	−0.0855 (37)
q_2^{H}	⋯	⋯	0.36 (9)
q_3^{H}	⋯	⋯	10.5 (15)
q_4^{H}	⋯	⋯	−135.8 (160)
No. of data	756	369	376
No. parameters	26	13	22
$\overline{\sigma_f}$	0.897	1.039	1.035

[a]Value taken from Ref. 22.
[b]Generated from Eq. (16); its uncertainty is the same as that for $\mathcal{D}_e(X)$.

provement in $\overline{\sigma_f}$ they yield is unlikely to be physically significant. Moreover, the direct potential fits require substantially fewer parameters than the converged parameter fits for the same systems.

For the CuH case, it is interesting to note that the copper atom electronic isotope shift coefficients determined in the two methods, $\tilde{\delta}_{0,0}^{\mathrm{Cu}}(\mathrm{A}) = 1.19(\pm 0.04)$ cm^{-1} and $\tilde{u}_0^{\mathrm{Cu}}(\mathrm{A}) = 1.23(\pm 0.07)$ cm^{-1} are essentially equivalent, corresponding to an A-state electronic isotope shift from ^{63}CuH (or D) to ^{65}CuH (or D) of $0.037(\pm 0.003)$ cm^{-1} [see Eqs. (14) and (16)]. As noted earlier, this means that the metal atom contribution to the zero point energy correction due to higher-order semiclassical effects is either negligible or essentially identical in the two electronic states.

IV. SUMMARY

Fourier transform emission spectroscopy has been used to record ground state vibration–rotation spectra for various isotopomers of CuH, AgH, and AuH. In spite of the intense background thermal emission of the high temperature carbon tube furnace, it was possible to record high resolution infrared emission spectra for these systems. These results were combined with high resolution pure rotational spectra for CuH and CuD and optical spectra for CuD and AuH taken from the literature, and analyzed using two types of combined-isotopomer analysis: Dunham-type parameter fits including atomic mass dependent B–O–B type isotopic corrections, and direct fits to potential energy functions with atomic mass dependent adiabatic and nonadiabatic radial correction functions. The two approaches yield fits of essentially equal quality; the slightly larger $\overline{\sigma_f}$ values associated with the direct potential fits are a reflection of the constraints imposed by the greater physical reality of that approach. Moreover, the direct potential fits are much more compact (requiring only $\frac{1}{2}$ to $\frac{2}{3}$ as many parameters), and are expected to yield much more reliable extrapolations to higher-J states.

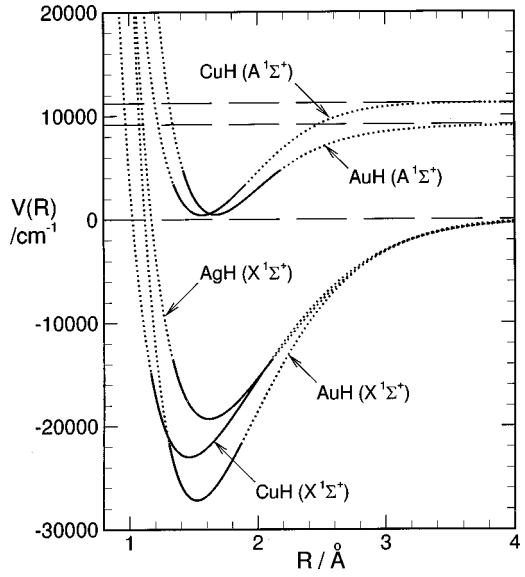

FIG. 6. Potential energy curves determined from our direct potential fits to multi-isotopomer data sets for the coinage metal hydrides. The solid curve segments indicate the intervals spanned by the data set used in the analysis.

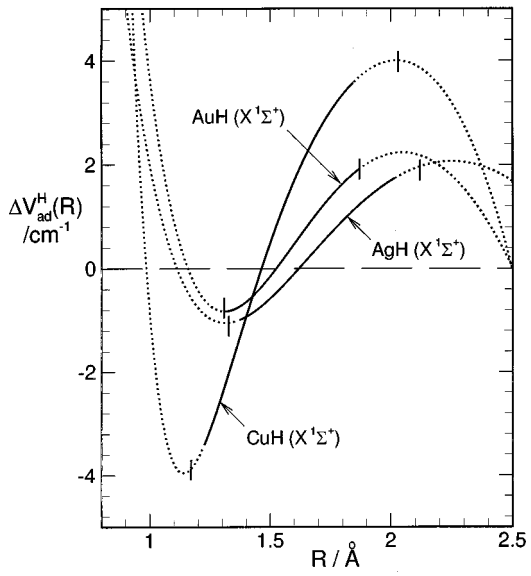

FIG. 8. Born–Oppenheimer breakdown adiabatic potential correction functions determined from multi-isotopomer direct potential fits. The solid curve segments indicate the intervals spanned by the data for the minority isotopomer, which determine this quantity, and the vertical bars indicate the bounds on the (in general broader) intervals on which the potential function for the dominant isotopomer is defined.

On the other hand, generating such predictions from the results of the potential fit approach is somewhat less convenient, as it would require a user to run a radial Schrödinger-solver program, rather than simply substitute quantum numbers into analytic expressions. At the same time, the agreement between the values of the A–X electronic isotope shift from ^{63}CuD to ^{65}CuD provides gratifying confirmation of the physical consistency of the two approaches.

One of the objectives of the present work was to examine the magnitude and nature of B–O–B type corrections for a family of related hydrides. Figures 7 and 8 show that the ground state hydrogenic B–O–B radial correction functions have the same magnitude and qualitative behavior, and the greater magnitude of the CuH A-state centrifugal correction function in the upper segment of Fig. 7 is readily understood in terms of the stronger nonadiabatic coupling expected for an excited electronic state. Within the parameter-fit results one can compare the magnitudes of individual B–O–B cor-

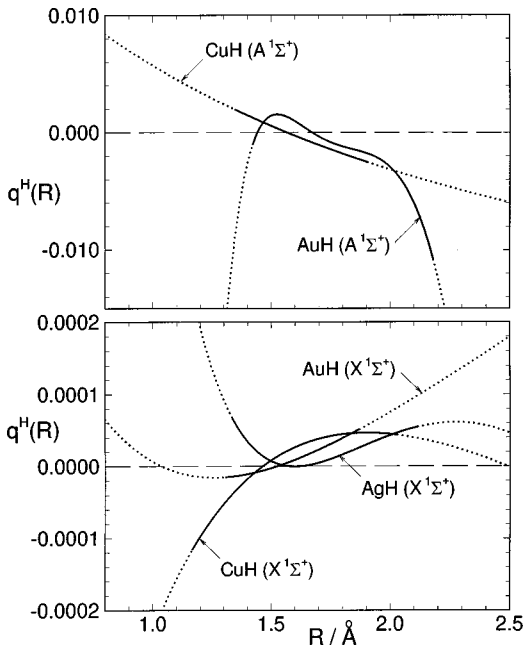

FIG. 7. Centrifugal Born–Oppenheimer breakdown correction functions determined from multi-isotopomer direct potential fits. The solid curve segments indicate the intervals spanned by the data set used here, and are the same as those associated with the corresponding potentials of Fig. 6.

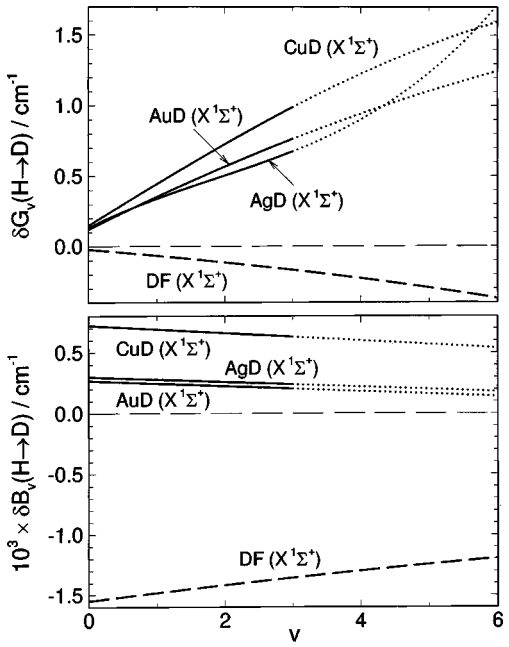

FIG. 9. Contribution of B–O–B type corrections to the H→D isotope shift of the vibrational energies (upper segment) and inertial rotational constants (lower segment) of the ground electronic state of the coinage metal deuterides (solid curves, dotted in extrapolation region) and of ground state DF (dashed curves, from results of Ref. 42).

rection expansion parameters, but it is more enlightening to examine the contribution of these corrections to the differences between the properties of different isotopomers. To this end, Fig. 9 plots the B–O–B type contributions to the vibrational energies and inertial rotational constants of each deuteride; these are calculated by substituting the appropriate $\delta_{l,m}^{H}$ parameters and masses into the second expansion in Eq. (2). Once again, we see that these corrections have the same magnitude and qualitative behavior in these three systems. It is interesting to note, however, that while of roughly the same magnitude the analogous corrections for HF determined in Ref. 42 (dashed curves in Fig. 9) have the opposite sign. However, a discussion of the characteristic magnitude and nature of these corrections is beyond the scope of the present work.

ACKNOWLEDGMENTS

We are grateful to Dr. C. Amiot for providing us with a listing of the transition frequencies measured in the electronic spectrum of AuH. We thank the Natural Sciences and Engineering Research Council of Canada (NSERC) for financial support, and the Petroleum research Fund of the American Chemical Society for partial support.

[1] *Transition Metal Hydrides*, edited by A. Dedieu (VCH, New York, 1992).
[2] C. Jaschek and M. Jaschek, *The Behavior of Chemical Elements in Stars* (Cambridge University Press, Cambridge, U.K., 1995).
[3] J. A. Coxon and P. G. Hajigeorgiou, J. Mol. Spectrosc. **139**, 84 (1990).
[4] J. A. Coxon and P. G. Hajigeorgiou, J. Mol. Spectrosc. **142**, 254 (1990).
[5] J. A. Coxon and P. G. Hajigeorgiou, J. Mol. Spectrosc. **150**, 1 (1991).
[6] R. Frerichs, Z. Phys. **20**, 170 (1923).
[7] Ö. Hauge, Astron. Astrophys. **10**, 73 (1971).
[8] R. S. Wojslaw and B. F. Perry, Astrophys. J., Suppl. **31**, 75 (1976).
[9] U. Ringström, Ark. Fys. **32**, 211 (1966).
[10] U. Ringström, Can. J. Phys. **98**, 2291 (1968).
[11] B. Grundström, Z. Phys. **98**, 128 (1935).
[12] C. M. Brown and M. L. Ginter, J. Mol. Spectrosc. **80**, 145 (1980).
[13] T. Heimer, Naturwissenschaften **23**, 372 (1935).
[14] M. A. Jeppesen, Phys. Rev. **50**, 445 (1936).
[15] W. T. M. L. Fernando, L. C. O'Brien, and P. F. Bernath, J. Mol. Spectrosc. **139**, 461 (1990).
[16] R. S. Ram, P. F. Bernath, and J. W. Brault, J. Mol. Spectrosc. **113**, 451 (1985).
[17] R. S. Ram, P. F. Bernath, and J. W. Brault, J. Mol. Spectrosc. **113**, 269 (1985).
[18] S. P. Beaton and K. M. Evenson, J. Mol. Spectrosc. **142**, 336 (1990).
[19] T. D. Varberg and K. M. Evenson, J. Mol. Spectrosc. **164**, 531 (1994).
[20] T. Okabayashi and M. Tanimoto, Astrophys. J. **487**, 463 (1997).
[21] E. Bengtsson and E. Olsson, Z. Phys. **72**, 163 (1931).
[22] K. P. Huber and G. Herzberg, *Constants of Diatomic Molecules* (Van Nostrand, Toronto, 1979).
[23] H. Birk and H. Jones, Chem. Phys. Lett. **161**, 27 (1989).
[24] R-D. Urban, H. Birk, P. Polomsky, and H. Jones, J. Chem. Phys. **94**, 2523 (1991).
[25] T. Ziegler, J. G. Snijders, and E. J. Baerends, J. Chem. Phys. **74**, 1271 (1981).
[26] U. Ringström, Nature (London) **198**, 981 (1963).
[27] U. Ringström, Ark. Fys. **27**, 227 (1964).
[28] C. E. Fellows, M. Rosberg and A. P. C. Campos, R. F. Gutteres, and C. Amiot, J. Mol. Spectrosc. **185**, 420 (1997).
[29] P. Pyykkö, Chem. Rev. **88**, 563 (1988).
[30] P. Schwerdtfeger, M. Dolg, W. H. E. Schwarz, G. A. Bowmaker, and P. D. W. Boyd, J. Chem. Phys. **91**, 1762 (1989).
[31] P. J. Hay, W. R. Wadt, L. R. Kahn, and F. W. Bobrowicz, J. Chem. Phys. **69**, 984 (1978).
[32] G. J. Jansen and B. A. Hess, Chem. Phys. Lett. **160**, 507 (1989).
[33] Y. S. Lee and A. D. McLean, J. Chem. Phys. **79**, 3392 (1982).
[34] G. Jansen and B. A. Hess, Z. Phys. D **91**, 1762 (1989).
[35] A. Pizlo, G. Jansen, B. A. Hess, and W. von Neissen, J. Chem. Phys. **98**, 3945 (1993).
[36] A. J. Sadlej, J. Chem. Phys. **95**, 2614 (1991).
[37] V. Kello, A. J. Sadlej, J. Chem. Phys. **95**, 8248 (1991).
[38] P. F. Bernath, *Spectra of Atoms and Molecules* (Oxford University Press, Oxford, 1995).
[39] R. J. Le Roy, J. Mol. Spectrosc. **191**, 223 (1998).
[40] G. Audi and A. H. Wapstra, Nucl. Phys. A **565**, 1 (1993).
[41] See AIP Document No. E-PAPS: EJCPSA6-110-022924 for ASCII files containing listings of the data used in the present analyses. E-PAPS document files can be retrieved free of charge from AIP's FTP server (http://www.aip.org/pubservs/paps.html) or from ftp.aip.org in the directory /epaps/. For further information, e-mail: paps@aip.org or fax 516-576-2223.
[42] R. J. Le Roy, J. Mol. Spectrosc. **194**, 189 (1999).
[43] A. H. M. Ross, R. S. Eng, and H. Kildal, Opt. Commun. **12**, 433 (1974).
[44] P. R. Bunker, J. Mol. Spectrosc. **68**, 367 (1977).
[45] J. K. G. Watson, J. Mol. Spectrosc. **80**, 411 (1980).
[46] Requests for program DSPARFIT (Diatomic Singlet Parameter Fits), by R. J. Le Roy, should be sent by electronic mail to leroy@UWaterloo.ca.
[47] J. K. G. Watson, J. Mol. Spectrosc. **45**, 99 (1973).
[48] H. G. Hedderich, M. Dulick, and P. F. Bernath, J. Chem. Phys. **99**, 8363 (1993).
[49] A. Šurkus, Chem. Phys. Lett. **279**, 236 (1997).
[50] M. Born and J. R. Oppenheimer, Ann. Phys. (Leipzig) **84**, 457 (1927).
[51] Exceptions are the treatment of the potentials and adiabataic potential correction functions in Refs. 49, 52, and 53.
[52] J. A. Coxon and R. Colin, J. Mol. Spectrosc. **181**, 215 (1997).
[53] J. A. Coxon and P. Hajigeorgiou, J. Mol. Spectrosc. **193**, 306 (1999).
[54] P. Hajigeorgiou and R. J. Le Roy, in *49th Ohio State University International Symposium on Molecular Spectroscopy* (Columbus, Ohio, 1994), paper WE04.
[55] Program DSPOTFIT (Diatomic Singlet Potential Fits), by J. Y. Seto and R. J. Le Roy, will be available on request from *leroy@UWaterloo.ca* in the near future.
[56] K. Smith, *The Calculation of Atomic Collision Processes* (Wiley-Interscience, New York, 1971), Chap. 4.
[57] C. E. Moore, *Atomic Energy Levels As Derived From the Analyses of Optical Spectra* (National Bureau of Standards, Washington, DC, 1952), Vol. 2.
[58] C. E. Moore, *Atomic Energy Levels As Derived From the Analyses of Optical Spectra* (National Bureau of Standards, Washington, DC, 1958), Vol. 3.
[59] Although unreported, this also occurs for a number of the direct-fit potentials found in the literature.